Contrib Mineral Petrol (1994) 115:313–322

Contributions to Mineralogy and Petrology

Anhydrous partial melting of an iron-rich mantle I: subsolidus phase assemblages and partial melting phase relations at 10 to 30 kbar

Constance M. Bertka[1,2*] **and John R. Holloway**[2,3]

[1] Geophysical Laboratory, Carnegie Institution of Washington, USA
[2] Department of Geology, Arizona State University, USA
[3] Department of Chemistry, Arizona State University, USA

Received May 21, 1992 / Accepted April 15, 1993

Abstract. Anhydrous partial melting experiments, at 10 to 30 kbar from solidus to near liquidus temperature, have been performed on an iron-rich martian mantle composition, DW. The DW subsolidus assemblage from ≤ 5 kbar to at least 24 kbar is a spinel lherzolite. At 25 kbar garnet is stable at the solidus along with spinel. The clinopyroxene stable on the DW solidus at and above 10 kbar is a pigeonitic clinopyroxene. Pigeonitic clinopyroxene is the first phase to melt out of the spinel lherzolite assemblage at less than 20°C above the solidus. Spinel melts out of the assemblage about 50°C above the solidus followed by a 150° to 200°C temperature interval where melts are in equilibrium with orthopyroxene and olivine. The temperature interval over which pigeonitic clinopyroxene melts out of an iron-rich spinel lherzolite assemblage is smaller than the temperature interval over which augite melts out of an iron-poor spinel lherzolite assemblage. The dominant solidus assemblage in the source regions of the Tharsis plateau, and for a large percentage of the martian mantle, is a spinel lherzolite.

Introduction

Primary melt compositions are liquid compositions in equilibrium with their source region, that is, unmodified by fractionation or other subsequent melting processes. Previous partial melting studies have explored the effect of source region characteristics on primary melt production for numerous conditions; i.e. pressures of up to 140 kbar, near solidus to near liquidus temperatures, carbonate-free, carbonate-rich, anhydrous, H_2O oversaturated and H_2O undersaturated, and mixed volatiles (e.g. Kushiro 1968; Green 1973; Millhollen et al. 1974; Mysen and Kushiro 1977; Eggler 1978; Presnall et al. 1978; Jaques and Green 1980; Takahashi and Kushiro 1983; Takahashi 1986; Falloon et al. 1988). Synthetic starting compositions derived from models for the Earth's primitive upper mantle or natural lherzolite nodules were used in those studies. These compositions are iron-poor, with mg#s greater than 87 (mg# = atomic [Mg/(Mg + Fe^{2+})*100]). The mg#s of naturally occurring lherzolites are largely within the range 87 to 92 (Maaloe and Aoki 1977), but individual samples with mg#s as low as 83 have been found (Jackson and Wright 1970). The occurrence of iron-rich primitive volcanic rocks, ferropicrites, also suggests that more iron-rich local source regions exist (Hanski and Smolkin 1989). A source region whose iron-rich character may have exerted a strong control over magma production on a planetary scale is the martian mantle. The purpose of our study has been to provide partial melting data for an iron-rich mantle. The composition we chose for study was a model martian mantle composition.

Models for the bulk composition of Mars predict a mantle whose major element abundances are similar to the Earth's except for iron (Table 1). Proposed models for the martian mantle are iron-rich with mg#s ranging from 75 to 80 (McGetchin and Smyth 1978; Morgan and Anders 1979; BVSP 1981; Goettel 1983; Dreibus and Wanke 1985). These models are either based on cosmochemical arguments (e.g. equilibrium condensation model), or derived by the addition of iron to a terrestrial mineral assemblage. With one exception (Dreibus and Wanke 1985), they predict the abundance of iron from calculations of mantle density.

Calculations of mantle density depend on knowledge of the mean moment of inertia of Mars (Johnston et al. 1974; Johnston and Toksoz 1977; Okal and Anderson 1978; Goettel 1981). This value is poorly constrained and recently an estimate which would result in a more Earth-like mantle iron abundance has been proposed (Bills 1989). However, there is a group of petrologically and geochemically distinct meteorites, the SNCs (shergottites, nakhlites, chassignites), that constrain the martian composition independent of estimates of mantle density, if

* *Present address:* Geophysical Laboratory, Carnegie Institution of Washington, 5251 Broad Branch Rd. N.W., Washington, DC 20015-1305, USA

Correspondence to: C.M. Bertka

Table 1. Bulk mantle compositions

	MARS			EARTH		
	McGetchin & Smyth[a]	Goettel[b]	DW Dreibus & Wanke[c]	KLB[d]	Pyrolite[e]	PHN1611[f]
wt %						
SiO_2	40.04	45.07	44.40	44.48	45.0	43.70
TiO_2	0.63	–	0.14	0.16	0.2	0.25
Al_2O_3	3.14	3.26	3.02	3.59	4.4	2.75
FeO	18.85	15.07	17.90	8.10	7.6	10.05
MnO	0.12	–	0.46	0.12	0.11	0.13
MgO	33.22	32.08	30.20	39.22	38.80	37.22
CaO	2.73	3.03	2.45	3.44	3.4	3.26
Na_2O	0.51	1.40	0.50	0.30	0.4	0.33
K_2O	0.12	0.12	–	0.02	–	0.14
P_2O_5	0.05	–	0.16	0.03	–	–
Cr_2O_3	0.38	–	0.76	0.31	0.5	0.28
NiO	0.18	–	–	0.25	–	–
Total	99.59	100.03	99.99	100.02	100.41	98.11
mg #	75.8	79.1	75.0	89.6	90.1	86.8

[a] McGetchin and Smyth (1978) after Morgan and Anders (1979); [b] Goettel (1983); [c] Dreibus and Wanke (1985); [d] Takahashi (1986); [e] Green et al. (1979); and [f] Mysen and Kushiro (1977)

Mars is the proposed parent body of the SNC meteorites (Wood and Ashwal 1981). Dreibus and Wanke (1985) used element correlations between measured ratios in SNCs and chondritic abundances to predict a SNC parent body with a mantle enriched in iron relative to the earth (Table 1). Our experiments are performed with the anhydrous SNC martian mantle composition DW (Dreibus and Wanke 1985).

Previous experimental work with an iron-rich martian composition in the system CaO-MgO-FeO-Al_2O_3-SiO_2 (CMFAS) indicated that a mantle with a mg# of 77 would have garnet stable as a subsolidus aluminous phase at a pressure 5 kbar lower than in the iron-free CMAS system, at the same temperature (Patera and Holloway 1982). Bertka and Holloway (1988) experimentally determined that the near solidus melt composition in equilibrium with an iron-rich (mg# = 78) garnet lherzolite source region at 23 kbar is a picritic alkali basalt. Subsolidus mineralogy and partial melting products of an iron-rich mantle have also been predicted from theoretical studies. By using a mantle norm algorithm, McGetchin and Smyth (1978) predicted the mineral assemblage of the martian mantle. A similar approach was taken by Stolper (1980) who projected iron-rich bulk compositions into experimentally determined phase regions of the CMAS system. Wood and Holloway (1982) used thermodynamic calculations in the Na_2O-CMFAS system to predict subsolidus assemblages. In the theoretical studies, the primary melt compositions produced from partial melting of the assemblages were modelled after terrestrial primary melts in equilibrium with the same assemblage.

The melting reaction which takes place at the solidus of a mantle composition is determined by the coexisting mineral assemblage (e.g. Mysen and Kushiro 1977). The success of modelling iron-rich partial melting processes after results from iron-free or iron-poor systems depends on the accuracy with which we can predict the effect of iron on the coexisting mineral assemblage of a multiphase, multicomponent mantle system. The normative approaches assume a simple substitution of FeO for MgO in solid solution minerals and melts. The thermodynamic calculations, due to a lack of appropriate data, must often approximate complex solution behavior with simple models. The results of our study demonstrate the significance of pigeonitic clinopyroxene, a phase previously overlooked by both the normative and thermodynamic based approaches, to partial melting processes in an iron-rich mantle. Previous theoretical studies of iron-rich mantle assemblages that do not include pigeonitic clinopyroxene in their determination of stable mineral assemblages or partial melt compositions are incomplete.

The results of our study are presented in two parts. In this paper, the near solidus mineral compositions for the DW mantle from 10 to 30 kbar and details of the melting phase relations from 10 to 20 kbar, that is the temperature interval over which the mineral phases melt out of the assemblage, are reported. These results are compared with previous partial melting studies with more Mg-rich compositions. In part II, Bertka and Holloway (1993a, this volume), primary melt and coexisting mineral compositions for increasing degrees of partial melting in the spinel lherzolite field at 15 kbar are reported. These results are also compared with previous partial melting studies with more Mg-rich compositions. Finally, implications for basalt petrogenesis on Mars as well as for iron-rich terrestrial source regions on Earth are discussed.

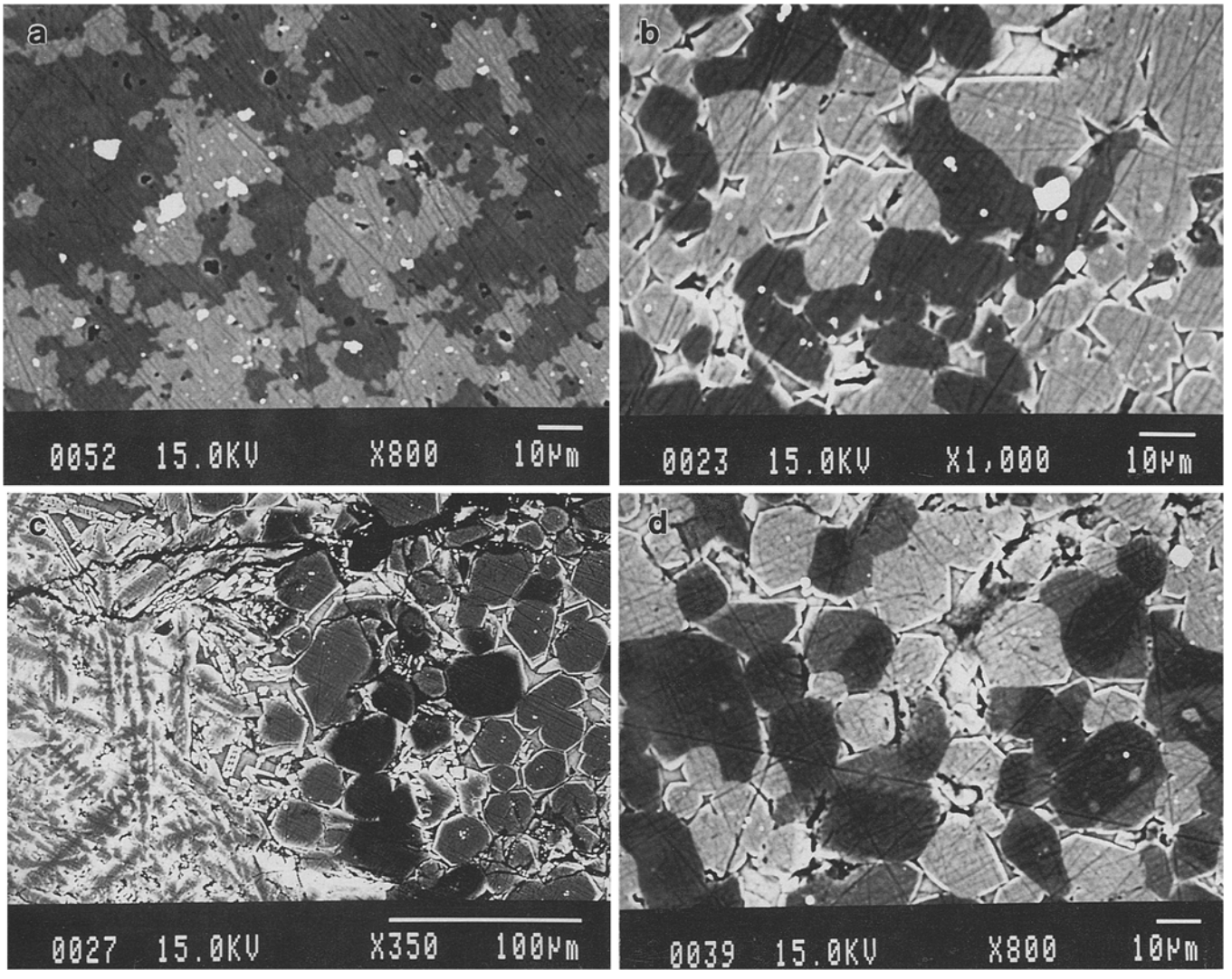

Fig. 1a–d. Backscattered electron images of run products at 15 kbar. Individual mineral phases are distinguished by a change in gray scale. **a** Subsolidus run DWF-52 (1150°C). From lightest to darkest the mineral phases are spinel, olivine, clinopyroxene, and orthopyroxene. The smaller dark areas are void spaces. **b** Supersolidus run DWF-23 (1300°C). The outlines of individual grains are distinct and interstitial glass areas are present. From lightest to darkest the mineral phases are spinel, olivine and orthopyroxene. **c** Supersolidus run DWF-27 (1360°C). The outlines of individual grains are distinct and interstitial glass as well as glass + quench crystal areas (left side of figure) are present. From lightest to darkest the mineral phases are olivine, and orthopyroxene. **d** Supersolidus run DWF-39. The outlines of individual grains are distinct and interstitial glass areas are present. This charge was first equilibrated at 1400°C, well above the solidus, and then lowered to 1300°C, the solidus temperature. From lightest to darkest the mineral phases are spinel, olivine, clinopyroxene and orthopyroxene

Experimental approach

Solidus mineralogy and melting phase relations

The starting material for the partial melting experiments was a sintered oxide mix of the DW composition (Table 1). The DW composition was synthesized from spectroscopically pure oxides and carbonates ground under ethanol in an agate mortar for one hour, and reduced in a gas mixing furnace (1000°C, f_{O_2} at QFM-1 log unit) for 24 h. The sintered oxide mix was reground in a tungsten-carbide container to less than 5 µm. Experimental charges used to locate the pressure, near solidus temperatures, of the spinel to garnet transition were seeded with ~5 wt% garnet crystals in order to encourage garnet growth.

The solidus temperature of the DW composition from 10 to 20 kbar was located by comparing the appearance of backscattered electron images of a sequence of run products from increasing temperature (Fig. 1). Phase relations within 60°C of the solidus were bracketed with runs that had closely spaced, 20°C, temperature intervals. The melting temperature interval and the composition of the first phase to melt out of the assemblage were also confirmed with experiments initially run at temperatures well above the solidus and then lowered to solidus temperatures. Run duration varied from 48 h at near solidus temperatures to 1 h at near liquidus temperatures.

Oxygen fugacity

Approximately 10 mg of starting material was loaded into a 3.5 mm long graphite capsule and placed into an outer 3 mm O.D. platinum capsule that was welded closed. The inner graphite crucible weighed

approximately 20 mg and the outer Pt capsule 245 mg. The graphite crucibles were fired to red heat prior to loading the starting material and the loaded capsule, Pt + graphite + starting material, was heated to 400°C before being welded closed.

The inner graphite capsule helps prevent iron loss from the starting material to the outer platinum capsule (see also Bertka and Holloway 1988), and it constrains the maximum f_{O_2} of the charge (Holloway et al. 1992). By including a small, 0.15 mg, platinum wire in the charge, the f_{O_2} of the experiment could be calculated from the iron-quartz-fayalite buffer reaction, provided residual olivine and orthopyroxene were present (Bertka and Holloway 1988; Gudmundsson and Holloway 1988,1993):

$$O_2 + 2Fe + SiO_2 = Fe_2SiO_4$$

$$f_{O2} = \frac{a^{ol}_{Fe_2SiO_4}}{(K_{QFI})\,(a^{system}_{SiO_2})\,(a^{Pt}_{Fe})^2} \quad (1)$$

where

$a^{ol}_{Fe_2SiO_4}$ = activity of fayalite in olivine; defined by $(X^{ol}_{Fe_2SiO_4})^2$, analyzed mole fraction of fayalite in olivine;

K_{QFI} = equilibrium constant for the iron-quartz-fayalite buffer reaction after O'Neill (1987), with a pressure correction applied;

$a^{system}_{SiO_2}$ = activity of SiO_2 in the system, constrained by the coexistence of olivine and orthopyroxene after Nicholls (1977), with a pressure correction applied;

a^{Pt}_{Fe} = activity of iron in platinum; calculated from the product of X^{Pt}_{Fe}, the analyzed mole fraction of iron in the platinum wire and, γ^{Pt}_{Fe}, the activity coefficients of iron in platinum, determined by Gudmundsson and Holloway (1993).

Apparatus

Experiments were performed in an end-loaded, solid-media, piston-cylinder apparatus similar to that described by Boyd and England (1960) with a 0.5″ diameter cell assembly. The assembly consisted of a graphite tube furnace encased in a pyrex glass and outer NaCl sleeve. The sample container, centered in the hot spot of the graphite furnace, was surrounded by powdered alumina and the remaining space in the furnace was filled with AlSiMag spacers. All assembly materials, except the pyrex glass and NaCl sleeves, were fired to red heat prior to loading. The pyrex glass and NaCl sleeves were dried at 400°C.

Temperature was measured with a Pt-Pt10%Rh thermocouple that was encased in an 99.998% alumina insulator. The thermocouple junction was in contact with the top of the Pt capsule. No correction for the effect of pressure on the EMF output of the thermocouple was made. The temperature gradient across the length of a 3.5 mm capsule is $\leq$20°C (Boyd and England 1960, 1963). One experiment at 15 kbar, 1320°C, was run with temperature monitored by both a Pt-Pt10%Rh and a W5%Re-W26%Re thermocouple for 48 h. The difference between the two thermocouples was $\leq$15°C. No drift in the emf of the Pt-Pt90Rh10 thermocouple was recorded.

Pressure calibrations were based on the ferrosilite-quartz-fayalite reaction as determined by Bohlen et al. (1980). Pressure, with a friction correction of 10% applied to nominal values, has an uncertainty of $\pm$1 kbar. All experiments were performed using the hot, "piston out" method. The pressure was initially raised $\sim$10% higher than the required run pressure and maintained while the sample was brought to run temperature. Then the pressure was reduced to the desired value.

Analytical technique

Longitudinal sections of the experimental charges were mounted and polished. Backscattered electron images used to determine phase relations, and quanitative chemical analyses, were obtained at Arizona State University with a JEOL JXM-8600 electron microprobe equipped with both wavelength and energy dispersive detection systems. Operating conditions for the wavelength dispersive analyses were 15 kV accelerating potential and 10 nA beam current. A 2 μm diameter beam was used to analyze mineral phases. Standards for the analyses were natural oxides and silicates. The data were reduced using the Bence and Albee (1968) correction method.

The iron content of the platinum wires was analyzed with a 2 μm beam placed within 10 μm of the Pt wire-silicate interface.The iron content of the Pt wires increased by $\leq$1 wt% from core to rim. These data were reduced using the ZAF correction method (Reed 1975).

Approach to equilibrium

Experimental run times. One experimental test of an approach to equilibrium is to identify the minimum run time at which no further change in the composition of a phase occurs. Previous workers have shown that when natural minerals are used as the starting material for partial melting experiments the pyroxene grains are zoned, with out of equilibrium cores, even after run durations of several days (Takahashi and Kushiro 1983; Fujii and Scarfe 1985). The near solidus partial melting experiments of our study had run durations of 48 h. The pyroxene grains that grew from the sintered oxide mix have core compositions, after 48 h, that are nearly identical to those from an 8 day experiment. The only notable difference between the pyroxene compositions after 48 h and those after 8 days is the CaO

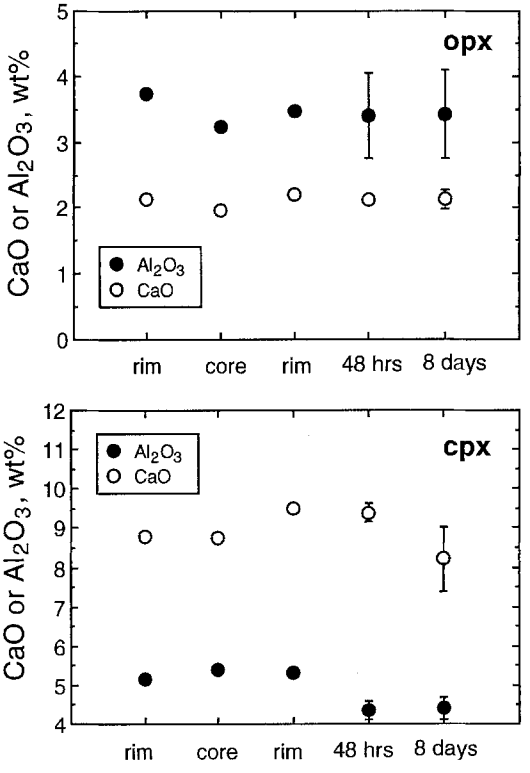

Fig. 2. CaO and Al_2O_3 abundances in pyroxenes in DW compositions run at 15 kbar and 1280°C. Shown are rim to rim analyses of single grains at 48 h and average core abundances of grains at 48 h and 8 days. The error bars on the analyses of core compositions are the standard deviation of abundances in those runs. Microprobe analyses of CaO and Al_2O_3 abundances in the pyroxenes are precise to 1% relative. The values plotted are represented by symbols that are larger than this analytical uncertainty

Table 2. 15 kbar near solidus spinel and clinopyroxene compositions

T° C	1280°		1280°		1280°		1280°		1300°		1300° (1400)[a]		1300° (1400)[a]	
Run Duration	48 h		8 days		48 h		8 days		48 h		48 h		48 h	
Phase	sp	$\pm 1\sigma$	sp	$\pm 1\sigma$	cpx	$\pm 1\sigma$	cpx	$\pm 1\sigma$	sp	$\pm 1\sigma$	sp	$\pm 1\sigma$	cpx	$\pm 1\sigma$
SiO_2	0.78	0.61	0.79	0.08	51.9	0.5	52.8	0.5	0.67	0.16	0.44	0.07	51.8	0.5
TiO_2	0.62	0.02	0.72	0.03	0.14	0.04	0.16	0.02	0.53	0.01	0.50	0.03	0.13	0.02
Al_2O_3	24.6	1.8	29.7	1.4	4.36	0.12	4.41	0.37	22.4	0.9	27.8	1.2	4.32	0.47
FeO	24.5	0.5	23.9	0	11.3	0.2	11.6	0.5	24.1	0.1	23.2	0.2	12.4	0.3
MnO	0.35	0.03	0.38	0.06	0.41	0.09	0.39	0.03	0.34	0	0.35	0.07	0.46	0.06
MgO	10.9	0.3	11.8	0	20.4	0.3	20.3	0.7	11.0	0.4	11.6	0.3	21.5	0.6
CaO	*		*		9.37	0.15	8.20	0.83	*		*		7.35	0.65
Na_2O	*		*		0.81	0.03	0.94	0.10	*		*		0.63	0.07
Cr_2O_3	38.3	1.2	32.7	1.4	1.34	0.10	1.25	0.15	40.9	1.2	36.2	0.9	1.36	0.26
mg #	44.3		46.8		76.2		75.7		44.9		47.1		75.6	

Reported analyses are normalized averages of at least three grains. Standard deviation is reported as absolute wt %
* Indicates that the measured value is zero within analytical precision
[a] This charge was first equilibrated at 1400° C and then lowered to 1300° C

abundance in clinopyroxene which decreases after 8 days by ~1 wt%, but still overlaps with the estimated range of core compositions from 48 h runs. Furthermore, the pyroxene grains are unzoned. In Fig. 2 the CaO and Al_2O_3contents from rim to rim, after 48 h, of a single orthopyroxene and clinopyroxene grain are shown, along with the average abundance of these oxides in pyroxene cores from experiments with run durations of both 48 h and 8 days, all at 15 kbar, 1280°C. The variation in CaO and Al_2O_3 abundance from rim to rim falls within or close to the range of average core values, except for Al_2O_3 in the clinopyroxene grain. Although this grain is not zoned in Al_2O_3,it has an Al_2O_3 content which falls outside the average Al_2O_3content of clinopyroxenes in this experimental charge. The mg#s of the analyses of the single clinopyroxene grain, from rim to rim, are identical; those of the single orthopyroxene grain, from rim to rim, differ by <1 mg#. We conclude that the subsolidus pyroxene grains have approached equilibrium by 48 h. Olivine compositions after 48 h and 8 days are also nearly identical, but after 8 days spinel compositions are 5 wt% richer in Al_2O_3, 6 wt% poorer in Cr_2O_3 and have higher mg#s, 46.8 vs 44.3 (Table 2).

Reversal experiments. The composition of the solidus spinel and clinopyroxene phases, and the melting interval of clinopyroxene, were confirmed with experimental charges that were first equilibrated at temperatures well above the solidus and then lowered in temperature to within 40°C of the solidus. The initial temperatures of these reversal experiments were not within the clinopyroxene or spinel stability fields. The clinopyroxenes and spinels that crystallized in these charges grew from the melt phase.

At near solidus temperatures the clinopyroxene compositions were virtually identical to the subsolidus clinopyroxenes that grew from the sintered oxide mix; SiO_2, FeO and MgO abundances differed by $\leq$1.2 wt%, Al_2O_3 abundances by $\leq$0.5 wt% and CaO abundances by $\leq$2.0 wt% (Table 2). The results of these experiments also confirmed that clinopyroxene melts out of the DW assemblage within 20°C of the solidus. Spinels that crystallized out of the melt at 40°C above the 15 kbar solidus had major element abundances similar to those which grew from the sintered oxide mix at the same temperature; FeO and MgO abundances differed by $\leq$1 wt%, Al_2O_3 and Cr_2O_3 abundances by $\leq$2.5 wt%. At temperatures closer to the solidus at 15 kbar, FeO and MgO abundances differed by $\leq$1 wt%, but Al_2O_3 and Cr_2O_3 abundances differed by 5 wt% (Table 2). At 10 kbar, near solidus temperatures, differences in Al_2O_3 and Cr_2O_3 abundances are even greater, up to 7.6 wt%. The spinels which crystallized out of the melt phase are judged to have a closer approach to equilibrium than those that grew from the sintered oxide mix, because the rate of cation diffusion is slower in crystalline phases than in a melt phase. Spinels, in some of the subsolidus runs at least, may not have reached equilibrium.

Fe/Mg partitioning. A comparison of previously calculated and measured Fe/Mg partition coefficients for the pairs olivine/orthopyroxene (ol/opx), and olivine/spinel (ol/sp), to the values experimentally determined in this study suggests that Fe-Mg exchange reactions between these pairs have approached equilibrium in our experiments. Sack and Ghiorso (1989) calculate ol/opx Fe/Mg K_D as a function of the mole fraction of fayalite in olivine, and of pressure and temperature. Like previously measured values, ours are lower, K_D = 1.1–1.25, than those calculated by Sack and Ghiorso (1989), K_D = 1.4–1.5, for similar mg# olivine-orthopyroxene pairs at the same pressure and temperature conditions. Our values compare favorably with other experimental values cited in Sack and Ghiorso (1989) from similar mg# olivine-orthopyroxene pairs, K_D = 1.2.

Olivine re-equilibrates faster to changes in melt Fe/Mg ratio than does orthopyroxene (Takahashi and Kushiro 1983), apparently because of differences in Fe-Mg diffusion rates in olivine and orthopyroxene. This difference aids in the identification of experimental charges that suffered iron loss when the melt phase came into contact with the Pt capsule through cracks in the graphite crucible. In these charges the orthopyroxenes retain an mg# that is lower than the equilibrium value. This results in ol/opx Fe/Mg partition coefficients that are too low. Likewise, in a reversal experiment, in which the charge is first equilibrated at a temperature higher than the final run temperature, the orthopyroxenes retain the higher temperature mg# resulting in ol/opx Fe/Mg partition coefficients that are too high. In our experiments iron loss was suspected if ol/opx Fe/Mg K_D was <1.1. When melt compositions were obtained in our partial melting experiments (Bertka and Holloway 1993a), mass balance calculations were performed to determine the mode of the phase assemblage. The results of these calculations are in agreement with those ol/opx K_Ds that suggest iron loss occurred. The calculated modes yield bulk compositions that match the starting DW composition, except for an iron deficiency. The amount of iron lost from the starting bulk composition in these experiments is between 2.5% and 12% relative; resulting in a minor change in bulk mg# from 75.0 to $\leq$77.4.

O'Neill and Wall (1987) derived an expression for the olivine-spinel Mg-Fe^{2+} exchange geothermometer. They did not define the uncertainty in the temperatures calculated from their geothermometer, but compared their values with the temperatures of experimentally equilibrated olivine-spinel pairs (Roeder et al. 1979). The calculated temperatures were up to 90°C too low. The geother-

Table 3. Experimental conditions and run products of partial melting experiments

Run #[a]	P kbar	T° C[b]	Time h	Run Products[c]
DWF-42	5	1125	48	ol + opx + cpx + sp + liq
DWF-50	10	1100	48	ol + opx + cpx + sp
DWF-12	10	1200	48	ol + opx + cpx + sp
DWF-41	10	1200 (1300)	24	ol + opx + cpx + sp
DWF-29	10	1220	48	ol + opx + cpx + sp + liq?
DWF-54	10	1220 (1300)	48	ol + opx + cpx + sp + liq
DWF-33	10	1240	48	ol + opx + sp + liq
DWF-32	10	1260	48	ol + opx + sp + liq
DWF-74	10	1280	48	ol + opx + sp + liq
DWF-9	10	1300	18.3	ol + opx + liq
DWF-2	10	1400	4	ol + opx + liq
DWF-5	10	1500	3	ol + opx + liq
DWF-14	10	1550	0.75	ol + liq
DWF-52	15	1150	48	ol + opx + cpx + sp
DWF-57	15	1150	168	ol + opx + cpx + sp
DWF-46	15	1200	40.5	ol + opx + cpx + sp
DWF-20	15	1280	48	ol + opx + cpx + sp
DWFC-61	15	1280	192	ol + opx + cpx + sp
DWF-23	15	1300	48.25	ol + opx + sp + liq
DWF-39	15	1300 (1400)	48	ol + opx + cpx + sp + liq
DWF-22	15	1320	48	ol + opx + sp + liq
DWF-55	15	1320 (1400)	48	ol + opx + sp + liq
DWF-25	15	1340	48	ol + opx + sp + liq
DWF-27	15	1360	48	ol + opx + liq
DWF-73	15	1400	24	ol + opx + liq
DWF-37	15	1500	5	ol + opx + liq
DWF-38	15	1550	5	ol + liq
DWFS-47	18	1300	46	ol + opx + cpx + sp
DWF-8	20	1300	24	ol + opx + cpx + sp
DWF-13	20	1300	48	ol + opx + cpx + sp
DWFS-62	20	1320	48	ol + opx + cpx + sp
DWF-24	20	1340	48	ol + opx + cpx + sp
DWF-19	20	1360	48	ol + opx + sp + liq
DWF-26	20	1360 (1500)	48	ol + opx + sp + liq
DWF-21	20	1380	48	ol + opx + liq
DWF-58	20	1380 (1450)	48	ol + opx + sp + liq
DWF-6	20	1400	24	ol + opx + liq
DWF-1	20	1500	4	ol + opx + liq
DWF-30	20	1550	4	ol + liq
DWF-4	20	1600	2	ol + liq
DWFS-49	22	1350	48	ol + opx + cpx + sp
DWFS-69	24	1320	48	ol + opx + cpx + sp + gt
DWFS-64	26	1350	42	ol + opx + sp + gt + liq?
DWFS-66	28	1350	36	ol + opx + sp + gt + liq?
DWF-10	30	1300	24	ol + opx + cpx + sp + gt
DWF-31	30	1450	24	ol + opx + liq

[a] Starting material: DWF = DW oxide mix; DWFS = DW oxide mix + garnet seeds; DWFC = DW oxide mix + augite seeds
[b] Where initial temperature differs from final temperature initial temperature is given in parenthesis
[c] Run products: ol = olivine; opx = orthopyroxene; cpx = clinopyroxene; sp = spinel; gt = garnet; liq = melt

mometer may underestimate the temperature of equilibration. In general the temperatures calculated for the experimental olivine-spinel pairs of this study are also low, although most of the calculated temperatures differ from the experimental temperatures ≤ 50°C.

Results

The experimental conditions and the run products of the partial melting experiments are listed in Table 3. The melting phase relations of the DW bulk mantle composition are illustrated in Figure 3. The compositions of the near solidus minerals, at pressures of 10 to 24 kbar, are given in Table 4. The composition of near solidus liquids is a topic discussed in a separate paper (Bertka and Holloway 1993a).

Subsolidus mineral assemblages

The temperature at which melting began was estimated by comparing backscattered electron (BSE) images of the run products. Grain boundaries between subsolidus silicate minerals are marked only by a change in gray scale. However, if the assemblage began to melt then the outlines of individual grains are more distinct (Fig. 1).

The stable assemblage near the solidus, determined from 10 to 22 kbar, is a spinel lherzolite: olivine + orthopyroxene + clinopyroxene + spinel. In the BSE images spinel appears as bright euhedral grains, usually less than 10 μm in diameter. These grains have the lowest mg#s, ~45, and are chrome-rich, 31 to 38 wt% Cr_2O_3. The light gray crystals in the BSE images are olivines, mg# ~75. The olivine grains are 10 to 20 μm in diameter and are compositionally similar within any charge. The darkest, mg# ~78, and largest crystals, 10 to 35 μm, are orthopyroxene. They have Al_2O_3 contents of 2.4 to 5.4 wt% and CaO contents of 1.7 to 4.6 wt%. Clinopyroxene occurs in close association with orthopyroxene. Clinopyroxene has mg# ~76; in the BSE images it appears slightly lighter than orthopyroxene and it is difficult visually to distinguish the two minerals in subsolidus charges. The Al_2O_3 contents of the clinopyroxene are 3.2 to 5.8 wt% with CaO contents from 6.6 to 10.2 wt%. The evidence used to identify these clinopyroxene grains as pigeonitic clinopyroxene, and the implications of their presence for partial melting processes, are topics covered in a separate paper (Bertka and Holloway 1993b).

Garnet is stabilized between 20 and 24 kbar at 1320°C. At 24 kbar the cores of garnet seeds, mg# = 70, are rimmed by more iron-rich, mg# = 67, garnet overgrowths. At 20 kbar the final run product contains no evidence of the original garnet seed crystals. At 26 and 28 kbar, 1350°C, garnet seeds are also rimmed by more iron-rich garnet overgrowths. The location of the solidus at these pressures has not been bracketed with a sequence of subsolidus to near solidus runs. However, the experimental results are consistent with extrapolation from the lower pressure data and the work of Patera and Holloway (1982) on the pressure-temperature slope of the spinel to garnet transition in the CMFAS system, which suggests that garnet is stable at the solidus along with spinel between 24 and 26 kbar at ≤ 1350°C (Fig. 3). At and above 24 kbar the spinel grains are ≤ 3 μm in diameter and were not analyzed. The transition of the subsolidus assemblage to a plagioclase lherzolite was not observed to occur for composition DW at solidus temperatures, even at pressures as low as 5 kbar.

Melting phase relations of DW

With increasing degrees of melting above the solidus of DW, interstitial pools of melt form. These quench to glass

Table 4. Mineral compositions or near solidus assemblages

Run	10 kbar, 1220° C ($T_{solidus}$ = 1220° C ± 10)								15 kbar, 1280° C ($T_{solidus}$ = 1290° C ± 10)							
Phase	ol	±1σ	opx	±1σ	cpx	±1σ	sp	±1σ	ol	±1σ	opx	±1σ	cpx	±1σ	sp	±1σ
wt %																
SiO_2	38.0	0	52.7	1.0	52.7	0.3	0.59	0.26	37.4	0.2	53.2	0.5	51.9	0.5	0.43	0.06
TiO_2	*		0.16	0.08	0.15	0.02	0.74	0.05	*		0.06	0.05	0.14	0.04	0.62	0.02
Al_2O_3	0.17	0.09	3.92	1.52	3.56	0.36	28.2	0.4	0.09	0	3.40	0.62	4.36	0.12	24.6	1.8
FeO	22.9	0.3	13.4	0.7	12.4	0.3	23.8	0.2	22.7	0.1	13.1	0.2	11.3	0.2	24.5	0.5
MnO	0.40	0.04	0.43	0.05	0.43	0.02	0.38	0.07	0.42	0.02	0.38	0.03	0.41	0.09	0.35	0.03
MgO	38.0	0.7	25.2	2.5	21.2	0.4	11.2	0.2	38.9	0.2	26.6	0.2	20.4	0.3	10.9	0.3
CaO	0.31	0.04	3.12	1.45	7.83	0.74	*		0.28	0	2.13	0.02	9.37	0.15	*	
Na_2O	*		0.39	0.36	0.64	0.04	*		*		0.22	0.05	0.81	0.03	*	
Cr_2O_3	0.18	0.04	0.50	0.19	1.07	0.08	33.9	2.0	0.15	0.05	1.02	0.13	1.34	0.10	38.3	1.2
mg #	74.7		77.0		75.3		45.8		75.3		78.4		76.2		44.3	

Run	20 kbar, 1340° C ($T_{solidus}$ = 1350° C ± 10)								24 kbar, 1320° C ($T_{solidus}$ ≤ 1350° C)							
Phase	ol	±1σ	opx	±1σ	cpx	±1σ	sp	±1σ	ol	±1σ	opx	±1σ	cpx	±1σ	gt	±1σ
wt %																
SiO_2	37.8	0.4	52.1	0.4	52.2	1.0	0.67	0.08	38.9	0.2	53.4	0.2	52.6	0.3	41.3	0.6
TiO_2	*		0.13	0.01	0.10	0.02	0.68	0.02	*		0.13	0.01	0.15	0.04	0.21	0.09
Al_2O_3	0.13	0.01	4.54	0.44	4.19	0.85	30.2	0.1	0.12	0.04	4.87	0.18	5.17	0.63	21.0	0.2
FeO	22.9	0.1	13.3	0.4	12.4	0.3	25.1	0.3	21.9	0.4	13.0	0.1	10.6	0.4	13.4	0.2
MnO	0.46	0.02	0.41	0.05	0.46	0.03	0.39	0.06	0.41	0.06	0.37	0.02	0.43	0.01	0.68	0.04
MgO	38.3	0.5	25.9	0.5	21.8	0.8	11.8	0.03	38.2	0.5	25.0	0.4	18.9	0.8	15.1	0.4
CaO	0.27	0.01	2.08	0.05	6.77	0.13	*		0.20	0.02	2.10	0.19	9.54	0.69	5.30	0.07
Na_2O	*		0.34	0.03	0.95	0.09	*		*		0.39	0.02	1.30	0.06	*	
Cr_2O_3	0.13	0.18	1.14	0.13	1.13	0.33	31.1	0.5	0.20	0.04	0.83	0.12	1.24	0.01	2.93	0.13
mg #	74.9		77.6		75.8		45.5		75.6		77.5		76.0		66.7	

Reported analyses are normalized averages of at least three grains. Standard deviation is reported as absolute wt %
Spinels in 24 kbar assemblage not analyzed
* Indicates that the measured value is zero within analytical precision

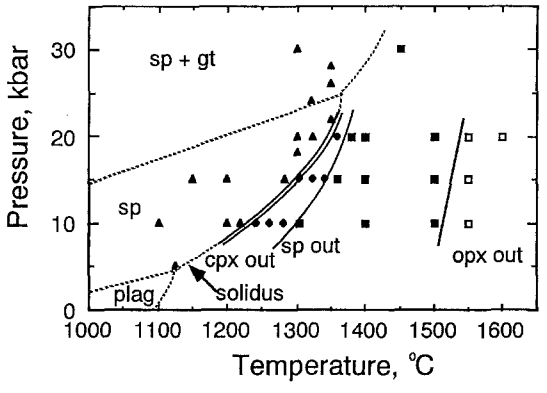

Fig. 3. Melting phase relations of the DW bulk mantle composition. The inferred location of the solidus, above 20 kbar and below 10 kbar, and subsolidus aluminous phase boundaries are shown with *dashed lines*. *Filled triangles*, ol + opx + cpx + sp ± gt; *filled diamonds*, ol + opx + sp + liq; *filled squares*, ol + opx + liq; *open squares*, ol + liq. Ol, olivine; opx, orthopyroxene; cpx, clinopyroxene; sp, spinel; gt, garnet; and liq, liquid. The cpx-out curve falls <20°C above the solidus. The slope of the subsolidus garnet-in curve is calculated from Patera and Holloway (1982)

and quench crystals which grow on the rims of stable crystals (Fig. 1). The first phase to melt out of the spinel lherzolite assemblage is clinopyroxene. Clinopyroxene is absent above the solidus except in two experimental charges one at 10 and one at 15 kbar (see Table 3). These charges were equilibrated at temperatures well above the solidus and then lowered in temperature to the solidus. Their clinopyroxene compositions are similar to those found in the subsolidus experimental charges. The data indicate that clinopyroxene melts out of the spinel lherzolite assemblage within 20°C of the solidus. As the degree of melting increases spinel is removed from the assemblage at about 50°C above the solidus. This change in phase relations is followed by a large temperature interval, 150°–200°C, where melts are in equilibrium with only olivine and orthopyroxene. In this interval the melt quenches to a mixture of quench crystals and glass (Fig. 1).

f_{O_2} calculations

The results of the f_{O_2} calculations at 10, 15 and 20 kbar are shown in a plot of log f_{O_2}, relative to NNO, versus temperature in Fig. 4. The f_{O_2} buffer curves for QFM,

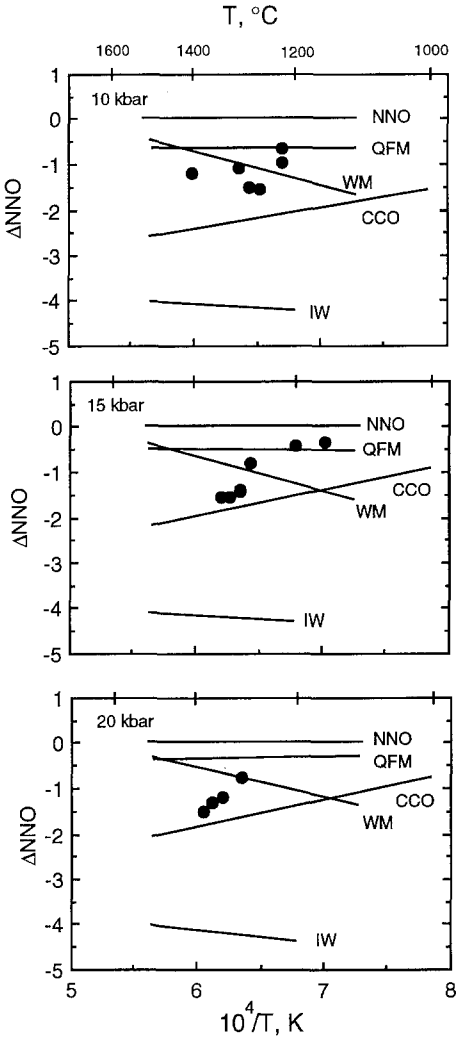

Fig. 4. Log f_{O_2} of partial melting experiments, relative to NNO, calculated from the QFI buffer reaction with the Pt-wire technique. f_{O_2} buffer curves: *QFM, IW, WM*, and *NNO*, Huebner (1971); *CCO*, Saxena and Fei (1987). *Filled circles*, f_{O_2} of partial melting experiments

WM, IW, NNO (Huebner 1971), and graphite-CO-CO_2 (Saxena and Fei 1987) are also shown. The results shown in Fig. 4 are plotted with a symbol size that represents an estimate of the total analytical uncertainty in $\log f_{O_2}$. Analytical uncertainty results in uncertainties of $a^{ol}_{Fe_2SiO_4} = \pm 3\%$, $a^{system}_{SiO_2} = \pm 6\%$, and $a^{Pt}_{Fe} = \pm 7\%$. A propagation of these uncertainties, assuming they are independent and random, suggests the calculated f_{O_2}s are accurate to within $\pm \sim 0.1$ log units. When alternative sources of thermodynamic data are used in the calculations, the calculated f_{O_2}s fall within 0.2 log units of the values shown in Fig. 4.

Thompson and Kushiro (1972) suggested that the use of graphite capsules in piston cylinder experiments would constrain the f_{O_2} of the charges to fall within the stability field of wustite. Holloway et al. (1992) point out that the presence of graphite in a capsule does not alone buffer the f_{O_2} but instead only places a limit on the maximum f_{O_2} obtainable, i.e. the value reached when a CO-CO_2 fluid phase is present. Without a fluid phase the f_{O_2} of the charge is dependent on the ferric/ferrous ratio of the starting material and the reaction between this material and the graphite capsule.

The calculated f_{O_2}s fall above the CCO buffer curve, a discrepancy which cannot be accounted for by analytical uncertainty alone. Gudmundsson and Holloway (personal communication) have also observed erroneously high f_{O_2} values using the Fe-Pt technique in the presence of graphite and believe this may be due to the effect of dissolved carbon on the activity coefficient of iron in Pt. If they are correct, the values reported here are subject to the same overestimate of f_{O_2}. However, within analytical uncertainty, most of the f_{O_2}s calculated for the partial melting experiments of this study fall within the stability field of wustite. The ferric iron content of the experimental charges was minimal.

Discussion

Subsolidus mineral assemblages and melting phase relations; iron-rich vs iron-poor source regions

Terrestrial spinel lherzolite KLB has a major element composition that is similar to the DW mantle except that KLB is iron-poor (mg# = 90) and 0.5 wt% and 1 wt% richer in Al_2O_3 and CaO, respectively (Table 1). The calculated modal abundances of clinopyroxene and spinel in the two mantle compositions are about the same, but the DW composition has more orthopyroxene and less olivine (Table 5).

The partial melting phase relations of KLB up to 30 kbar (Takahashi 1986) are shown in Fig. 5. KLB solidus temperatures are about 50°C higher than DW solidus temperatures at these pressures; this is a reasonable result because increasing the FeO/MgO ratio lowers the melting temperature of an assemblage. The stable subsolidus assemblage in both mantle compositions, from at least 10 to 25 kbar, is a spinel lherzolite, above 25 kbar, both compositions yield garnet lherzolite. This observation is an initially surprising result because increasing FeO increases the stability of garnet and lowers the pressure of the spinel- to garnet-lherzolite transition (e.g. Patera and Holloway 1982).

Patera and Holloway (1982) experimentally determined the pressure of the spinel- to garnet-lherzolite transition, at subsolidus temperatures, in an iron-rich martian mantle composition. At the same temperature, the transition occurred about 5 kbar lower in the iron-rich system (mg# = 76.8) than in the iron-free CMAS system. O'Neill (1981) calculated the effect of FeO on this transition. Based on these calculations we can predict

Table 5. Mantle modes

	KLB[a]	DW[b]
wt %		
Olivine	58	41.9
Orthopyroxene	25	37.9
Clinopyroxene	15	16.2
Spinel	2	4.0
Garnet	–	–

[a] Observed, Carter (1970)
[b] Calculated from 15 kbar, 1280° C assemblage

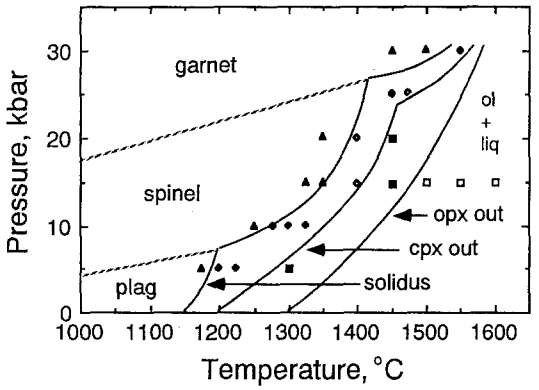

Fig. 5. Melting phase relations of the KLB bulk mantle composition after Takahashi (1986). Subsolidus aluminous phase boundaries are shown with *dashed lines*. *Filled triangles*, ol + opx + cpx + Al phase; *filled diamonds*, ol + opx + cpx + Al phase + liq; *open diamonds*, ol + opx + cpx + liq; *filled squares*, ol + opx + liq; and open squares, ol + liq. Ol, olivine; opx, orthopyroxene; cpx, clinopyroxene; sp, spinel; gt, garnet; and liq, liquid

that if the KLB and DW mantle compositions were similar, except for FeO abundances, then at a fixed temperature the transition would occur 3 kbar lower in the DW mantle than in the KLB mantle. However, the DW mantle composition is also richer in Cr_2O_3 (0.76 wt%) than KLB (0.31 wt%). O'Neill (1981) also calculated the effect of Cr_2O_3on the transition. If the only difference between the mantle compositions was Cr_2O_3 abundances, then the transition would occur 5 kbar higher in the DW mantle. The results of experimental work with peridotite mineral mixtures of varying Cr_2O_3 contents (MacGregor 1970) are in good agreement with these calculated results. The effects of increased Cr_2O_3 and FeO abundances in the DW mantle, over their abundance in the KLB mantle, cancel one another. The spinel to garnet transitions in these mantle compositions, at solidus temperatures, occur within ± 1 kbar of each other near a pressure of 25 kbar.

With increasing temperature above the spinel lherzolite solidus, clinopyroxene melts out of the KLB assemblage over a 60°C melting interval (Takahashi 1986); this is a much larger temperature interval than the melting interval for clinopyroxenes in DW, <20°C. As discussed in a separate paper (Bertka and Holloway 1993b), the difference in melting interval is attributed to the stability of pigeonitic clinopyroxene at the solidus of DW, rather than augite, the stable clinopyroxene at the solidus of KLB. A difference in clinopyroxene mineralogy results in a difference in the melting reaction at the solidus: Bertka and Holloway (1993b) describe the melting reaction by graphically illustrating the location of the partial melt in relation to the tetrahedron formed by the residual mantle minerals in a spinel–olivine–orthopyroxene–wollastonite compositional space. The melting reaction for KLB is Opx + Cpx + Sp = Ol + Liq; for DW the melting reaction is Cpx + Sp = Ol + Opx + Liq (Bertka and Holloway 1993b). In the DW mantle composition both olivine and orthopyroxene are in a reaction relation with the melt, whereas in the KLB composition, only olivine is in a reaction relation with the melt. With the onset of partial melting of the DW composition, the modal abundance of olivine and orthopyroxene in the partially melted assemblage increases. At the end of the first 60°C melting interval, both the DW and the KLB mantles consist of residual orthopyroxene and olivine. However, the orthopyroxene + olivine melting interval is much smaller in the KLB mantle, (~100°C) than in the DW mantle (~200°C).

Implications for basalt petrogenesis on Mars

At solidus temperatures, the transition from a spinel- to garnet-lherzolite assemblage occurs at a similar pressure in both the DW martian mantle composition and the KLB terrestrial mantle composition. Because the diameter of Mars is about 1/2 that of the Earth this pressure corresponds to a much greater depth in the martian mantle (~208 km) than in the Earth's mantle (~85 km). Therefore, the solidus assemblage over a large volume and mass percentage of the martian upper mantle, from ≤83 km to 208 km, is a spinel lherzolite.

One of the youngest volcanic centers on Mars is the Tharsis plateau (Greeley and Spudis 1981). The depth of magma source regions on Mars has been calculated from the relief of the central volcanoes in the Tharsis region (e.g. Carr 1976; Blasius and Cutts 1976; Thurber and Toksöz 1978). The calculated depths correspond to pressures of 13 to 30 kbar. Solomon and Head (1990) calculated the lithospheric thermal gradients underlying the volcanoes of the Tharsis region. Most of the calculated gradients intersect the DW solidus at pressures of 10 to 26 kbar. These results are in excellent agreement with the source region pressures predicted from the heights of the volcanoes. We conclude that the dominant near solidus assemblage in fertile source regions of the Tharsis plateau is a spinel lherzolite. The melt compositions produced by partial melting of an iron-rich spinel lherzolite are reported in part II of this study (Bertka and Holloway 1993a).

Acknowledgements. We thank Bjorn Mysen and James Tyburczy for their valuable comments on this manuscript. Rosamond Kinzler and John Longhi provided thoughtful reviews. James Clark provided expert technical assistance with the electron microprobe. The electron microprobe at Arizona State University was purchased with the aid of NSF grant EAR-8408163. This work was also supported by the Geophysical Laboratory of the Carnegie Institution of Washington where the first author was a predoctoral fellow, and through funding provided by the National Aeronautics and Space Administration's Graduate Student Researchers Program.

References

BVSP (Basaltic Volcanism Study Project) (1981) Geophysical and cosmochemical constraints on properties of mantles of the terrestrial planets. In: Basaltic volcanism on the terrestrial planets. Pergamon, New York, pp 633–699

Bence AE, Albee AL (1968) Empirical correction factors for the electron microanalysis of silicates and oxides. J Geol 76:382–403

Bertka CM, Holloway JR (1988) Martian mantle primary melts: an experimental study of iron-rich garnet lherzolite minimum melt composition. Proc Lunar Planet Sci Conf 18:723–739

Bertka CM, Holloway JR (1994a) Anhydrous partial melting of an iron-rich mantle II: primary melt compositions at 15 kbar. Contrib Mineral Petrol 115:323–338

Bertka CM, Holloway JR (1994b) Pigeonite at solidus temperatures: implications for partial melting. J Geophys Res (in press)

Bills BG (1989) The moments of inertia of Mars. Geophys Res Lett 16:385–388
Blasius KR, Cutts JA (1976) Shield volcanism and lithospheric structure beneath the Tharsis plateau, Mars. Proc Lunar Planet Sci Conf 7:3561–3573
Bohlen SR, Essene EJ, Boettcher AL (1980) Reinvestigation and application of olivine-quartz-orthopyroxene barometry. Earth Planet Sci Lett 47:1–10
Boyd FR, England JL (1960) Apparatus for phase-equilibrium measurements at pressures up to 50 kilobars and temperatures up to 1750°C. J Geophys Res 65:741–748
Boyd FR, England JL (1963) Effect of pressure on the melting of diopside, $CaMgSi_2O_6$, and albite, $NaAlSi_3O_8$, in the range up to 50 kilobars. J Geophys Res 68:311–323
Carter JL (1970) Mineralogy and chemistry of the earth's upper mantle based on the partial fusion-partial crystallization model. Bull Geol Soc Am 81:2021–2034
Carr MH (1976) The volcanoes of Mars. Sci Am 234:32–43
Dreibus G, Wanke H (1985) Mars: a volatile-rich planet. Meteoritics 20:367–382
Eggler DH (1978) Effect of CO_2 upon partial melting of peridotite in the system Na_2O-CaO-Al_2O_3-MgO-SiO_2-CO_2 to 35 kb, with an analysis of melting in a peridotite-H_2O-CO_2 system. Am J Sci 278:305–343
Falloon TJ, Green DH, Hatton CJ, Harris KL (1988) Anhydrous partial melting of a fertile and depleted peridotite from 2 to 30 kb and application to basalt petrogenesis. J Petrol 29:1257–1282
Fujii T, Scarfe CM (1985) Composition of liquids coexisting with spinel lherzolite at 10 kb and the genesis of MORBs. Contrib Mineral Petrol 90:18–28
Goettel KA (1981) Density of the mantle of Mars. Geophys Res Lett 8:497–500
Goettel KA (1983) Present constraints on the composition of the mantle of Mars. Carnegie Inst Washington Yearb 82:363–366
Greeley R, Spudis PD (1981) Volcanism on Mars. Rev Geophys Space Phys 19:13–41
Green DH (1973) Experimental melting studies on a model upper mantle composition at high pressure under water-saturated and water-undersaturated conditions. Earth Planet Sci Lett 19:37–53
Green DH, Hibberson WO, Jaques AL (1979) Petrogenesis of mid-ocean ridge basalts. In: McElhinny MW (ed) The earth: its origin, structure and evolution. Academic Press, New York, pp 265–295
Gudmundsson G, Holloway JR (1988) The activity coefficient of iron in platinum at 1400°C and from 1 atm to 20 kb (abstract). EOS Trans Am Geophys Union 69:1402
Gudmundsson G, Holloway JR (1993) Activity-composition relationships in the system Fe-Pt at 1300 and 1400°C and at 1 atm and 20 kbar. Am Mineral 78:178–186
Hanski EJ, Smolkin VF (1989) Pechenga ferropicrites and other early proterozoic picrites in the eastern part of the Baltic Shield. Precambrian Res 45:63–82
Holloway JR, Pan V, Gudmundsson G (1992) High pressure fluid-absent melting experiments in the presence of graphite: oxygen fugacity, ferric/ferrous ratio and dissolved CO_2. Eur J Mineral 4:105–114
Huebner JS (1971) Buffering techniques for hydroststic systems st elevated pressures. In: Ulmer GC (ed) Research techniques for high pressure and high temperature. Springer, New York, pp 123–178
Jackson ED, Wright TL (1970) Xenoliths in the Honolulu volcanic series, Hawaii. J Petrol 11:405–430
Jaques AL, Green DH (1980) Anhydrous melting of peridotite at 0–15 kb pressure and the genesis of tholeiitic basalts. Contrib Mineral Petrol 73:287–310
Johnston DH, McGetchin TR, Toksöz MN (1974) The thermal state and internal structure of Mars. J Geophys Res 79:3959–3971
Johnston DH, Toksöz MN (1977) Internal structure and properties of Mars. Icarus 32:73–84
Kushiro I (1968) Compositions of magmas formed by partial zone melting of the earth's upper mantle. J Geophys Res 73:619–634
Maaloe S, Aoki K (1977) The major element composition of the upper mantle estimated from the composition of lherzolites. Contrib Mineral Petrol 63:161–173
MacGregor ID (1970) The effect of CaO, Cr_2O_3, Fe_2O_3 and Al_2O_3 on the stability of spinel and garnet peridotites. Phys Earth Planet Interiors 3:372–377
McGetchin TR, Smyth JR (1978) The mantle of Mars: some possible geological implications of its high density. Icarus 34:512–536
Millhollen GL, Irving AJ, Wyllie PJ (1974) Melting interval of peridotite with 5.7 percent water to 30 kilobars. J Geol 82:575–587
Morgan JW, Anders E (1979) Chemical composition of Mars. Geochim Cosmochim Acta 43:1601–1610
Mysen BO, Kushiro I (1977) Compositional variations of coexisting phases with degree of melting of peridotite in the upper mantle. Am Mineral 62:843–865
Nicholls J (1977) The activities of components in natural silicate melts. In: Fraser DG (ed) Thermodynamics in geology. D Reidel, Dordrecht, Boston, pp 327–348
Okal EA, Anderson DL (1978) Theoretical models for Mars and their seismic properties. Icarus 33:514–528
O'Neill HStC (1981) The transition between spinel lherzolite and garnet lherzolite, and its use as a geobarometer. Contrib Mineral Petrol 77:185–194
O'Neill HStC (1987) Quartz-fayalite-iron and quartz-fayalite-magnetite equilibria and the free energy of formation of fayalite (Fe_2SiO_4) and magnetite (Fe_3O_4). Am Mineral 72:67–75
O'Neill HStC, Wall VJ (1987) The olivine-orthopyroxene-spinel oxygen geobarometer, the nickel precipitation curve, and the oxygen fugacity of the earth's upper mantle. J Petrol 28:1169–1191
Patera ES, Holloway JR (1982) Experimental determinations of the spinel-garnet boundary in a Martian mantle composition. Proc Lunar Planet Sci Conf 14, in J Geophys Res 87: A31–A36
Presnall DC, Dixon SA, Dixon JR, O'Donnell TH, Brenner NL, Schrock RL, Dycus DW (1978) Liquidus phase relations on the join diopside-forsterite-anorthite from 1 atm to 20 kb: their bearing on the generation and crystallization of basaltic magma. Contrib Mineral Petrol 66:203–220
Reed SJB (1975) Electron microprobe analysis. In: Cambridge Univ. Press, Cambridge
Roeder PL, Campbell IH, Jamieson HE (1979) A re-evaluation of the olivine-spinel geothermometer. Contrib Mineral Petrol 68:325–334
Sack RO, Ghiorso MS (1989) Importance of considerations of mixing properties in establishing an internally consistent thermodynamic database: thermochemistry of minerals in the system Mg_2SiO_4-Fe_2SiO_4-SiO_2. Contrib Mineral Petrol 102:41–68
Saxena SK, Fei Y (1987) High pressure and high temperature fluid fugacities. Geochim Cosmochim Acta 51:783–791
Solomon SC, Head JW (1990) Heterogeneities in the thickness of the elastic lithosphere of Mars: constraints on heat flow and internal dynamics. J Geophys Res 95:11073–11083
Stolper E (1980) Predictions of mineral assemblages in planetary interiors. Proc Lunar Planet Sci Conf 11:235–250
Takahashi E (1986) Melting of a dry peridotite KLB-1 up to 14 GPa: implications on the origin of peridotitic upper mantle. J Geophys Res 91:9367–9382
Takahashi E, Kushiro I (1983) Melting of a dry peridotite at high pressures and basalt magma genesis. Am Mineral 68:859–879
Thompson RN, Kushiro I (1972) The oxygen fugacity within graphite capsules in piston-cylinder apparatus at high pressures. Carnegie Inst Washington Yearb 71:615–616
Thurber CH, Toksöz MN (1978) Martian lithospheric thickness from elastic flexure theory. Geophys Res Lett 5:977–980
Wood BJ, Holloway JR (1982) Theoretical prediction of phase relationships in planetary mantles. J Geophys Res 87: A19-A30
Wood CA, Ashwal LD (1981) SNC meteorites: igneous rocks from Mars? Proc Lunar Planet Sci Conf 12:1359–1375

Editorial responsibility: T. Grove